RELATION BETWEENFIBRE DISTRIBUTION AND POST-CRACKING BEHAVIOUR IN STEEL FIBRE REINFORCED SELF-COMPACTING CONCRETEPANELS

Amin Abrishambaf *[1], Joaquim A. O. Barros[1] and Vitor M.C.F. Cunha[2]

[1] ISISE, Dep. Civil Eng., School Eng., University of Minho, Campus de Azurém 4800-058 Guimarães, Portugal

[2] ISISE, Eng. Department, School Science and Tech., University of Trás-osmontes e Alto Douro, 5001-801 Vila Real, Portugal

ABSTRACT

In this research, the influence of the fibre distribution and orientation on the post-cracking behaviour of steel fibre reinforced self-compacting concrete (SFRSCC) panels was studied. To perform this evaluation, SFRSCC panels were cast from their centre point. For each SFRSCC panel, cylindrical specimens were extracted and notched either parallel or perpendicular to the concrete flow direction, in order to evaluate the influence of fibre dispersion and orientation on the tensile performance. The post-cracking behaviour was assessed by both splitting tensile tests and uniaxial tensile tests. To assess the fibre density and orientation through the panels, an image analysis technique was employed across cut planes on each tested specimen. It is found that the splitting tensile test overestimates the post-cracking parameters. Specimens with notched plane parallel to the concrete flow direction show considerable higher post-cracking strength than specimens with notched plane perpendicular to the flow direction.

Keywords: Fibre reinforcement; Tensile properties; Rheology; Dispersion; Image analysis

* Author to whom the correspondence should be sent (amin.abrishambaf@yahoo.com).

1. INTRODUCTION

The addition of fibres to a cementitious matrix contributes mainly to the energy absorption capacity and crack control of structural elements, as well as to the enhancement of the load bearing capacity, particularly, in structural configurations with high support redundancy [1-2]. The fibre reinforcement mechanisms are mainly effective after concrete cracking initiation and, mostly, improve the post-cracking behaviour, due to the stress transfer provided by fibres bridging cracked sections. Crack opening in steel fibre reinforced concrete (SFRC) is counteracted by the bond stresses that develop at the fibres / matrix interface during the fibre pull-out. On the other hand, one of the most important properties of SFRC is its ability to transfer stresses across a cracked section rather uniformly, which nonetheless is dependent on the fibre reinforcement effectiveness, i.e. fibre properties (their strength, bond, and stiffness), and fibre orientation and distribution [3]. The stress transfer capability of fibres enhances mainly the composite's toughness, which is a parameter related to the energy absorption during monotonic or cyclic loading [4].

The dispersion and orientation of fibres in the hardened-state results from a series of stages that SFRC passes from mixing to hardening state, namely [5]: fresh-state properties after mixing; casting conditions into the formwork; flowability characteristics; vibration and wall-effect introduced by the formwork. Among these factors, wall-effects introduced by the moulds, and the properties of SFRC in the fresh state, especially its flowability, are the most important ones [5-7]. Having in mind that mechanical properties are significantly related to the fibre orientation and dispersion, which are affected by concrete's flow in the fresh state, it is important to control both those parameters (flowability and wall-effect) [8-10].

Application of steel fibres enhances the mechanical properties of concrete, but since all fibres cannot be aligned in the direction of the applied stress, the effectiveness of the fibres is dependent of the loading conditions, mainly on the directions of the principal tensile stresses. Moreover, it is shown that the fibre distribution's scatter in large scale elements may result in a significant inconsistency of the mechanical behaviour along the structural element. Therefore, it is feasible to expect an anisometric material behaviour for this kind of composite. In addition, the fibre efficiency depends on the orientation of the fibres towards the active crack plane. Some authors agree that in steel fibre reinforced self-compacting concrete (SFRSCC) the variability in the post-cracking parameters observed in bending tests, and also in uniaxial direct tensile tests, can be justified by the dispersion and alignment of the fibres [11-12]. Therefore, a significant research effort has been done to achieve better mechanical performances for SFRC by conditioning the distribution and orientation of the fibres [11, 13-15]. However, these effects should be considered for structural design, especially when fibre distribution and orientation affect significantly the mechanical properties of SFRC.

The main objective of this study is to connect experimentally the influence of the distribution / orientation of fibres, which are affected by flowability of concrete, to the post-cracking behaviour of SFRSCC developed and applied on laminar structures. To perform this evaluation SFRSCC panels were casted from their centre point. For each SFRSCC panel, cylindrical specimens were extracted and notched either parallel or perpendicular to the concrete flow direction to evaluate the effects of fibre dispersion and alignment on the tensile performance. The post-cracking behaviour was assessed by both splitting tensile tests and also uniaxial tensile tests. To characterize fibre density and orientation throughout the panels, an image analysis technique was employed across the cut plane of each tested specimen.

2. EXPERIMENTAL RESEARCH

2.1 Concrete mixture

The constituent materials used in the composition of the SFRSCC were: Portland cement CEM 42.5 R (C), water (W), superplasticizer Sika® 3005 (SP), limestone filler, crushed granite aggregate, fine and coarse sand, and hooked-end steel fibres (length, l_f, of 33 mm; diameter, d_f, of 0.55 mm; aspect ratio, l_f / d_f , of 60 and a yield stress of 1100 MPa). The adopted mix proportions are shown in Table 1, where W/C is the water/cement ratio. To evaluate the properties of SFRSCC in the fresh state, the inverted Abrams cone slump test was performed according to EFNARC recommendations [16]. An average spread of 670 mm was achieved without sign of segregation of the constituents. The compressive strength and Young's modulus were determined using cylinders of 150 mm diameter and 300 mm height after 28 days of moist curing in a climate chamber (3 cylinders for each test). The average compressive strength (f_{cm}) and the average value of the Young's modulus (E_{cm}) were 47.77 MPa (7.45 %) and 34.15 GPa (0.21 %), respectively, where the values in parentheses represent the coefficient of variation.

2.2 Specimens

According to [17], casting a slab from its centre assures better mechanical behaviour compared to the other casting methods. Therefore this direction of casting was selected for the production of two SFRSCC panels. The dimensions of the panels are 1600× 1000 mm^2 in plan, with 60 mm of thickness. The fresh concrete was poured directly from the mixing-truck by using a U-shape channel at the centre of the mould from a height of 60 cm. The influence of fibre dispersion and orientation within the panel on the post-cracking behaviour was assessed by means of splitting (Brazilian type) and direct tensile tests. Twenty-three specimens were extracted from each panel along the concrete flow directions, according to the scheme represented in Fig. 1. In this figure the pale dash lines with arrows represent the supposed concrete flow directions. When the driling operations were performed, the panels were already in their harden-mature phase. The hatched cores were used for executing splitting tensile tests, while the rest were used for uniaxial tensile tests. In the splitting tensile test, to localize the specimen's fracture, two notches with a 5 mm depth were executed on cores' opposite sides. The influence of the crack orientation towards the concrete flow was assessed in two distinct directions. By assuming θ as the angle between the notched plane and the direction of the concrete flow, the notch plane is designated parallel for $\theta = 0^{\circ}$ or perpendicular for $\theta = 90^{\circ}$. Since the core scheme was maintained for both panels, for each core location there are two cores with perpendicular notch direction. This will enable to evaluate the influence of fibre orientation at a certain distance from the casting position on the stress-crack width (σ-w) relationship. For instance, θ of A1 specimen is 90° and 0° in panels A and B, respectively.

The remaining cores extracted from the cast panels were sawn out from cylinders of 150 mm diameter and 60 mm thickness according to the schematic representation shown in Fig. 2. Twenty two prismatic specimens with dimensions of 110×102×60 mm^3 were produced for the uniaxial tensile test program. Following the same notching procedure for the splitting test specimens, the prismatic specimens were notched according to parallel ($\theta = 0^{\circ}$) and perpendicular ($\theta = 90^{\circ}$) directions to the expected concrete flow. The notch was executed in the four lateral faces of the specimen, at its mid-height, with a thickness of 2 mm and a depth of 5 mm. Special care was given to this operation to produce a notch with precise and uniform dimensions, and also to ensure the notch plane becomes perpendicular to the direction of the applied stress.

2.3 Test setup

2.3.1 Splitting tensile test

To determine the *σ*-*w* relationship representative of the SFRSCC panel, splitting tensile tests based on the ASTM C-496 [18] were executed. The tests were carried out in displacement-control using an universal testing rig with a bearing capacity of 150 kN. The tests were performed with a relatively low displacement rate of 0.001 mm/s enabling to obtain a stable response once the crack process is initiated. This low displacement rate was kept constant throughout the test execution. An external displacement transducer positioned on the actuator that measured the vertical deformation of the specimen was used to control the test.

Each specimen was positioned between two rigid supports and subjected to a diametral compressive line load applied along the thickness of the specimen. It is assumed that this applied load induces a constant tensile stress in the central part of the notched plane; therefore the results are expected to be close to the uniaxial tensile test results [19]. The test setup is depicted in Fig. 3. In each specimen five linear variable diferential transducers (LVDTs) were applied according to the configuration schematically represented in Fig. 3a and 3b to record crack opening along the notched plane. The support aluminium plates of each LVDT guaranttee the register of the opening of the two opposed faces of the notch, Fig. 3c. To assess if unsymmetric crack oppening occurs, due to fibre segregation during the casting procedure, two LVDTs were located at the specimen's bottom surface, while the others were fixed on the top surface of the specimen.

2.3.2 Uniaxial tensile test

After sawing and notching operations, each specimen was carefully cleaned with pressurized air and acetone. Then, two loading steel plates were glued with epoxy to the top and bottom surfaces of the specimen and subjected to a uniform pressure during three days enabling the perfect alignment of the loading plates. Sikadur®-30 Normal epoxy adhesive was used for this purpose.

A high stiff universal testing rig with a bearing capacity of 1000kN was used to execute the uniaxial tensile tests, Fig. 4a. This test was carried out in close-loop displacement control by averaging the signals of four displacement transducers installed on the two opposite faces of the specimen (top and bottom of the panel), Fig. 4b. Distinct displacement rates were applied during the test according to the following procedure: 0.005 mm/min up to a displacement of 0.05 mm, 0.02 mm/min up to a displacement of 0.1 mm, 0.08 mm/min up to a displacement of 0.5

mm/min and finally, 0.1 mm/min until the completion of the test. The adopted displacement rates comply with the recommendations of RILEM TDF-162 [20].

2.3.3 Assessment of fibre distribution and orientation

To find out correlations between fibre distribution parameters and mechanical properties, such as, residual stresses and absorption energy, it is quite important to determine fibre dispersion and fibre orientation parameters. There are several methods for assessing the fibre distribution and orientation in fibre reinforced composites, namely: tomography (CT-scan) [21], image analysis [22], x-ray method [17], electrical resistivity [17], ultrasound and quantitative acoustic emission technique [23], and magnetic approach [24]. Among these methods, image analysis technique was chosen due to its simplicity and relatively low cost of the necessary equipment.

The adopted procedure for fibre detection comprised four main steps. Firstly, the fracture surface of the specimen was grinded. To enhance the reflective properties of the steel fibres, the surface was polished and cleaned with acetone. Secondly, a colored image of this surface was taken using a high resolution digital photograph camera. Afterwards, the obtained image was processed using ImageJ [25] software to recognize steel fibres. These steps are depicted in Fig. 5. This method was also adopted by other researchers [13, 26, 27]. After analyzing the images, the acquired data was processed, and the total number of fibres intersecting the plane (N_T^f), number of effective fibres (N_{eff}^f), orientation of each fibre (θ), and segregation factor (ξ_{seg}) were obtained. Each parameter will be defined subsequently.

The number of fibres per unit area, N^f , is the ratio between the total number of fibres counted in an image, N_T^f , and the total area of the image, A:

$$N^f = N_T^f / A \tag{1}$$

The effective fibres, N_{eff}^f , per unit area are those that had the hooked end deformed, and those that have fractured. The number of effective fibres was determined by visual inspection of the fracture surfaces.

The assessment of the fibre orientation degree at a certain plane can be given by a fibre orientation factor, η_θ, Eq.(2). Based on an image analysis procedure of cut planes, the ellipses' axis of an intersecting fibre can be easily determined. Therefore, in this method, the orientation factor η_θ can be regarded as an average orientation towards a certain plane surface.

$$\eta_\theta = \frac{1}{N_T^f}.\sum_{i=1}^{N_T^f} \cos\theta_i \qquad (2)$$

In Eq. (2) N_T^f is the total number of fibres that can be determined by counting all the visible ellipses and circles at the cross section, θ is the out-plane angle that is defined as the angle between the fibre's longitudinal axis and a vector orthogonal to the plane.

The last analysed parameter was the fibre segregation along the gravity direction, determined from:

$$\xi_{seg} = \frac{1}{h.N_T^f}.\sum_{i=1}^{N_T^f} \overline{y} \qquad (3)$$

where $\overline{y}$ is the coordinate in the Y axis of the fibre's gravity centre, and h is the height (or depth) of the analysed cross-section. To calculate the location of the steel fibres gravity centre, an average value of the coordinates in the Y axis of entire fibres should be determined in the analysed cross-section. The ξ_{seg} parameter can assume values between 0 (segregation at the top of the cross-section) and 1(segregation at the bottom of the cross-section). In a SFRC with ideal fibre distribution, ξ_{seg} is 0.5.

3. ANALYSIS OF RESULTS AND DISCUSSION

Table 2 includes the residual stresses and toughness parameters for different average crack widths. In this table, σ_{peak} is the stress at peak load that represents the maximum tensile stress; $\sigma_{0.3}$, σ_1 and σ_2 are the residual stresses at a crack opening width of 0.3, 1 and 2 mm, respectively; G_{F1} and G_{F2} are the dissipated energy up to a crack width of, respectively, 1 and 2 mm. Additionally, the coefficient of variation, CoV, and the characteristic values for a confidence interval of 95%, $k_{95\%}$, are also included. From the results it is noticed that the influence of the notch orientation towards the concrete's flow on the post-peak behaviour of the material is quite high. The series with a notch inclination of θ = 0º shows higher residual tensile stresses and also larger dissipated energy than the specimens with θ = 90º. This variation in the post-cracking parameters could be ascribed to a preferential orientation of the fibres at the fracture surface. As it will be discussed in more detail further ahead, during the casting stage, fibres have the tendency to be aligned perpendicular to the direction of concrete flow, maybe due to a uniform radial velocity profile as also observed by [14, 17]. Therefore, for the specimens with the notched plane parallel to the flow direction, more fibres are almost perpendicular to the crack plane and, consequently, a higher number of fibres intersect more effectively the fracture surface. Previous research on the fibre pullout behaviour has revealed that fibre reinforcement effectiveness is almost the same for a fibre orientation towards the normal to the crack plane lower than 30 degrees [28].

3.1 Splitting tensile test

Fig. 6 depictsthe nominal stress – crack opening mouth displacement relationship, σ – w, for specimens extracted from distinct panels' locations. The envelope and the correspondent average curves are presented in this figure. The crack width was determined by averaging the recorded displacements of the 5 LVDTs installed on the faces of each specimen, see Fig. 3. The nominal tensile stress at the centre of the specimen was obtained from the following equation [29]:

$$\sigma = \sigma_{SP} = \frac{2F}{\pi D L} \quad (4)$$

where F is the applied line load, D is the diameter of the cylinder (150 mm) and L is the thickness of the net area in the notched plane (50 mm). Although the applicability of Eq. (4) is arguable in the softening phase of SFRSCC, since it is based on the theory of elasticity, it will be used to estimate the tensile stress at the cracked surface, as adopted by other researchers [19, 26, 30].

The σ - w responses are almost linear up to the stress at crack initiation. Up to this stress level, the displacements recorded by the LVDTs represent the transversal elastic deformation of the SFRSCC volume between the supports of the LVDTs (Fig. 3c). Therefore, the deformability during this first phase should have been removed from the σ - w response, but due to its negligible value this was not executed. After crack initiation, the σ - w response is nonlinear up to peak load. Once the peak load was attained, the load has smoothly decreased being visible a softening response. Note that, for the specimens with the notch perpendicular to the flow direction (θ = 90º), the peak stress was equal to the stress at crack initiation.

Generally, the σ – w responses exhibited a relatively high scatter. In SFRSCC, this type of scatter is generally high, even in specimens from the same casting and with the same testing conditions, due to the high dependence of the post-cracking behaviour on the fibre distribution and orientation. Since the specimens were extracted from distinct slab locations, at different distances from the casting point, a high scatter was expected. In fact, the viscous nature of SFRSCC affects the distribution of the concrete constituents along the flow process.

Fig. 7 shows the $\sigma - w$ relationships at the two sides of the specimens, representative of the top and bottom surfaces of the panels. Additionally the average curve is also included. The crack width was determined by averaging the LVDTs readouts installed on each surface. As it is shown from the results, the LVDTs on the bottom surface registered a lower value of the crack opening than the ones at the top surface for the same load level. This means that the crack opened asymmetrically, which is justified by the fibre tendency to segregate along the depth of the element [31]. The effect of fibre segregation was slightly higher in the θ = 90º series. This aspect will be corroborated and discussed in a subsequent section with the determination of a fibre segregation factor.

3.2 Uniaxial tensile test

Fig. 8 depicts the average and envelope stress-crack width (σ-w) curves regarding to each series. For both series (θ = 0° and 90°), the σ-w curve is almost linear up to the load at crack initiation. The concrete tensile strength was approximately 2.7 MPa. Once the tensile strength is attained, the stress suddenly decreases up to a crack width about 0.07 mm. Beyond this crack width, θ = 0° and 90° series behave in a completely distinct way. A semi-hardening and a plateau responses are observed for the θ = 0° and 90°series, respectively. Regarding the θ = 0° series, Cunha *et al.*[28] have analyzed the micromechanical behaviour of hooked end fibres by performing fibre pull-out tests, and have verified that after a fibre sliding of nearby 0.1 mm, the fibre reinforcement mechanism is mainly governed by the hook plastification during the fibre pull-out process. Therefore, in this series, fibres start to be pulled-out slowly being observed a semi-hardening response. Afterwards, in θ = 0° specimens, up to the crack width of about 0.6 mm, a plateau response is observed, which is then followed by a smooth drop in the residual stress. From experimental and analytical analysis, it was verified [32-33] that the average orientation angle value of the active fibres bridging a leading crack is about 35°. According to fibre pull-out tests performed by Cunha et al. [34], in the case of the inclination angle of 30° with the load direction, fibre rupture is the most predominant failure mode between the slip range of 0.6-1.0 mm. In fact, during the uniaxial tensile test execution, after peak load is attained the sound of the fibre rupturing was clearly noticeable that caused a rapid drop in the value of the load. This was confirmed after analysing the fracture surface by visual inspection.

In the case of θ = 90˚, some specimens shown a pseudo-hardening behaviour, especially those located nearby the centre of the panel. After this pseudo-hardening behaviour, it is observed a small plateau followed by a reduction of the residual stress beyond a crack width of about 0.9 mm, which corresponded to the rupture of the fibres.

The pre-peak branch shows very low scattering, while in the post-cracking phase the scatter of the response was considerably higher. In the elastic phase the contribution of fibres is rather negligible. After crack initiation, the role of the fibres becomes more important in bridging the stresses across the crack surfaces. This process depends significantly on how fibres are distributed and oriented through the matrix, which means the scattering observed in the post-cracking phase is highly influenced by the variation of the fibre dispersion and orientation amongst different specimens. Hence, for the latter series it is more logical to categorize the σ-w relationships based on distinct fibre orientation factor and distribution, which will be discussed in the next section.

3.3 Comparison of the results

Fig. 9 shows the relationship between the ratio of the splitting tensile post-cracking parameters, σ_{SPLT}, $G_{F\ SPLT}$ and the uniaxial tensile post-cracking parameters, σ_{UTT}, $G_{F\ UTT}$ for the crack width corresponding to σ_{peak} that is known as w_{peak}, and at crack width values of 0.3, 1.0 and 2.0 mm. In Fig. 9(a) for θ = 0° series, w_{peak} does not represent the same value for splitting tensile test (0.44 mm) and uniaxial tensile test (0.34 mm), therefore this interval is represented as a hatched vertical strip. For the θ = 90° series this problem is not crucial since σ_{peak} coincides with the stress at crack initiation, which happened for a negligible crack opening (w_{peak}). The data plotted in Fig. 9(a) clearly shows that σ_{SPLT} is larger than σ_{UTT} for almost all w (*CMOD*) values considered except at $w = w_{\text{peak}}$ for the $\theta=90$˚ series. Therefore, splitting tensile test overestimates the tensile residual strength. The average tensile stress at peak load for the splitting and uniaxial tensile test was 4.39 and 3.30 MPa for θ = 0° specimens, and 2.47 and 2.72 MPa for θ=90°series. With the increase of the crack opening, the $\sigma_{SPLT} / \sigma_{UTT}$ ratio became higher, since in the softening phase fibres started being mobilized as they bridge the stresses across the crack surfaces.

Fig. 9(b) depicts the relationship between the energy absorbed during the fracture process in both test setups, up to a crack width of 0.3, 1 and 2 mm. Both series presented a similar tendency, an increase of G_f with the crack width was observed. On the other hand, in the average term, for 0.3 mm crack width, the $G_{F\ SPLT} / G_{F\ UTT}$ ratio is 1.33 and 1.94 for θ = 0˚ and θ = 90˚ series, respectively. This ratio has increased up to 1.62 and 2.05 for 2 mm crack width, respectively, for θ = 0˚ and θ = 90˚ series.

3.4 Fibre distribution and orientation

Table 3 includes the fibre distribution parameters obtained by image analysis on the plane surface (see Fig. 10) of the specimens subjected to uniaxial tension test. Within each panel, by assuming the casting point as origin, specimens with the same distance from casting origin are presented in the same row. For each studied distance, the number of fibres was assessed in two perpendicular planes (θ = 0° and 90°, Fig. 1). From the analysed results, N^f and N^f_{eff} were significantly higher at the specimens with θ = 0º, approximately 80% and 254 %, respectively, when comparing to specimens with θ = 90º. This high variation of the fibre distribution in two perpendicular directions could be ascribed to a preferential fibre alignment influenced by the concrete's flowability. Moreover, the probability that a random section plane crossing a single fibre is a function of the fibre's length (*L*), diameter (*D*), and also the angle that the it makes with the section plane (fibre orientation factor) [35]. Since all the fibres have the same aspect ratio, the value of *D* and *L* are constant, therefore the probability function depends on the fibre orientation factor. On the other hand, the higher orientation factor leads to a higher probability of a single fibre intersecting a section plane. Concerning the fibre segregation factor, the obtained average values of ξ_{seg} for the studied cross sectional planes were slightly higher than 0.5, approximately 7.6 to 14.6%. The obtained values are coherent with the σ - w curves depicted in Fig. 7, since it justifies why the value of the crack opening determined in the bottom surface of the cores in θ = 90° specimens is lower than the other series. Thus, for the studied self-compacting concrete composition, slightly fibre segregation towards the bottom of the specimen due to the gravity action was observed. In terms of the fibre orientation factor, η_θ, specimens from series θ = 0° had higher values than the θ = 90° series, which means that the fibres are more aligned perpendicular to the fracture plane in the θ = 0° series.

Fig. 11 depicts orientation profiles obtained for the average orientation factor of each series separately. In this figure, the distribution of the orientation angle through the cut plane was studied for each specimen separately and the experimental results were compared to Gaussian distribution. According to this study, the distribution of the orientation angle follows closely a Gaussian distribution. Laranjeira*et al.* [36] had already obtained similar conclusion. Based on this method, an Excel spreadsheet was developed in order to determine the probability density distribution of fibre orientation. As it is expected, θ = 0° specimens show a distribution shifted to the left side, which means fibres have a tendency to be oriented more perpendicular to the cut plane (crack plane). On the other hand, the θ = 90° distribution is slightly transferred to the right side and more fibres tend to be aligned parallel to the cut plane (crack plane). Regarding to the comparison with theoretical orientation values for a two-dimensional distribution, *2/π*, [37] and a three-dimensional isotropic uniform random fibre distribution, 0.5, [38] θ = 0° specimens had a very different distribution profile, whereas orientation profile in θ = 90° series has matched with 2D fibre random distribution perfectly. Consequently, in the case of casting panels from the centre, for θ = 0° series the assumption of a 2D or 3D uniform random fibre distribution is far apart from the reality. In the present case, the distribution is prominently influenced by the placing conditions and concrete flowability.

Based on the obtained results, since in the casting process of the panels, particularly from the centre, the wall effects are negligible, the flow velocity is uniform and diffuses outwards radially from the casting point, see Fig. 12. Therefore, fibres have a tendency to orient perpendicular to the concrete flow direction. As a consequence, in the θ = 0° series the SFRSCC presented a semi-hardening response due to the high number of effective fibres with favourable orientation, while in the θ = 90° series, since fibres were rotated due to the concrete flow velocity, the number of the effective fibres is reduced and lower residual strengths are observed.

Fig. 13 depicts the relationship between the fibre density measured at the notched fracture surfaces after performing direct tensile test and the distance from the casting point. In this figure $N_{f_{\parallel}}$ and $N_{f_{\perp}}$ are, respectively, the fibre density at a crack plane parallel and perpendicular to the concrete flow. As it is expected, due to the proper viscosity of the concrete, a good homogeneity and dispersion of the fibres were achieved all over the panels, and a higher fibre density was obtained in the fracture surfaces in the alignment of the concrete flow.

The σ - w relationships previously obtained (see Fig. 8) have shown a high scatter due to the distinct fibre distributions. In order to reduce the scatter of the results and also study the influence of η_θ and N_{eff}^{f}, the σ - w relationships were separated in three different categories, see Fig.14. From this figure, it is concluded that the post-cracking parameters depend not only in η_θ but also in N_{eff}^{f}. Fig. 15 clearly shows that by increasing the orientation factor, the number of the effective fibres tends to rise exponentially.

4. CONCLUSION

In the present work, the influence of fibre distribution / orientation on the tensile performance of steel fibre reinforced self-compacting concrete (SFRSCC) was characterized by performing splitting and uniaxial tensile tests on cored specimens extracted from different panel locations.

Fibre distribution and orientation have a strong impact on the tensile behaviour of specimens drilled from the panels. In the case of the series with crack plane parallel to the concrete flow direction (θ = 0°), specimens shown significantly higher post-cracking parameters than the other studied case with a perpendicular crack plane to the flow direction (θ = 90°). When a panel is cast from the centre, fibres have a tendency to line up perpendicularly to the radial flow, mainly due to the uniform flow profile velocity that diffuses outwards radially from the centre of the panel. Hence, the total number of the effective fibres intersecting the parallel crack plane (θ = 0°) was higher than the one registered in the orthogonal crack plane (θ = 90°).

The probabilistic distribution of the orientation angle through a cut plane follows closely a Gaussian distribution. By determining the probability density function of fibre orientation for each series separately, it is found that for θ=0° specimens the assumption of 2D and 3D uniform random fibre distribution is completely far apart from the reality, while θ = 90° series follows a pattern very close to the theoretical 2D random fibre distribution.

Splitting tensile tests tend to overestimate the post-cracking parameters, but clearly capture all phases of post-cracking response. Moreover, the splitting tests have presented a lower scattering of the results when compared to the uniaxial tensile test. The load at crack initiation step was not influenced by fibres; both tests estimated similar tensile strengths. The post-peak stresses and energy absorption parameters obtained from the splitting tensile tests, especially, the energy absorption parameters have shown a reasonable correlation with the ones obtained from the uniaxial tensile tests.

AKNOWLEDEGMENT

The studies reported in this paper are part of the research project LEGOUSE (QREN, project nº 5387). This project is co-supported by FEDER through COMPETE program ("*Programa Operacional Factores de Competitividade*"). The materials were supplied by Radmix and Maccaferri (fibres), SECIL (cement), SIKA and BASF (superplasticizers), Omya Comital (limestone filler), and Pegop (Fly ash).

REFERENCES

[1] ACI 544–1R, State-of-the-art report on fiber reinforced concrete, Technical report, American Concrete Institute, 2002.

[2] P.N. Balaguru, S.P. Shah, Fiber reinforced cement composites, McGraw-Hill Inc., New York, 1992.

[3] L. Vandewalle, D. Dupont, Bending test and interpretation, test and design methods for steel fibre reinforced concrete - Background and Experiences, RILEM publication PRO 31, Bagneux, (2003) 1-14.

[4] RILEM TC162-TDF, Test and design methods for steel fibre reinforced concrete: Bending test, Mater. Struct. 33 (2000) 75-81.

[5] F. Laranjeira, Design-oriented constitutive model for steel fiber reinforced concrete, PhD thesis, Universitat Politècnica de Catalunya, 2010.

[6] D. Dupont, L. Vandewalle, Distribution of steel fibres in rectangular sections, Cem. Concr. Compos. 27 (2005) 391-398.

[7] L. Martinie, P. Rossi, N. Roussel, Rheology of fiber reinforced cementitious materials: classification and prediction, Cem. Concr. Res. 40 (2010) 226-234.

[8] L. Ferrara, A. Meda, Relationships between fibre distribution, workability and the mechanical properties of SFRC applied to precast roof elements, Mater. Struct. 39 (2006) 411-420.

[9] W. Pansuk, H. Sato, Y. Sato, R. Shionaga, Tensile behaviours and fibre orientation of UHPC, Proceedings of Second International Symposium on Ultra High Performance Concrete, Kassel, Germany (Kassel University Press), (2008) 161-168.

[10] S.W. Kim, S.T. Kang, J.J. Park, G.S. Ryu, Effect of filling method on fibre orientation and dispersion and mechanical properties of UHPC, Proceedings of Second International Symposium on Ultra High Performance Concrete, Kassel, Germany (Kassel University Press), (2008)185-192.

[11] M.C. Torrijos, B.E. Barragan, R.L. Zerbino, Placing conditions, mesostructural characteristics and post-cracking response of fibre reinforced self-compacting concretes, Constr. Build. Mater. 24 (2010) 1078-1085.

[12] B.E. Barragan, R. Gettu, M.A. Martin, R.L. Zerbino, Uniaxial tension test for steel fibre reinforced concrete-a parametric study, Cem. Concr. Compos. 25 (2003) 767-777.

[13] S.T. Kang, J.K. Kim, The relation between fibre orientation and tensile behavior in an Ultra High Performance Fibre Reinforced Cementitious Composites (UHPFRCC), Cem. Concr. Res. 41 (2011) 1001-1014.

[14] B. Boulekbache, M. Hamrat, M. Chemrouk, S. Amziane, Flowability of fibre-reinforced concrete and its effect on the mechanical properties of the material, Constr. Build. Mater. 24 (2010) 1664-1671.

[15] N., Ozyurt, T.O. Mason, S.P. Shah, Correlation of fibre dispersion, rheology and mechanical performance of FRCs, Cem. Concr.Compos. 29 (2007)70-79.

[16] EFNARC, The European guidelines for self-compacting concrete, May 2005.

[17] S.J. Barnett, J.F. Lataste, T. Parry, S.G. Millard, M.N. Soutsos, Assessment of fiber orientation in ultra high performance fibre reinforced concrete and its effects on flexural strength, Mater. Struct. 43 (2010) 1009-1023.

[18] ASTM C496, Standard test method for splitting tensile strength of cylindrical concrete specimens, Annual Book of ASTM Standards, American Society of Testing Materials,2004.

[19] S. Carmona, A. Aguado, New model for the indirect determination of the tensile stress-strain curve of concrete by means of the Brazilian test, Mater. Struct. (2012) 1-13.

[20] RILEM TC 162-TDF, Test and design methods for steel fibre reinforced concretes: Uniaxial tension test for steel fibre reinforced concrete, Mater. Struct. 34(1):3(6) 2001.

[21] P. Stähli, R. Custer, J.G.M van Mier, On flow properties, fibre distribution, fibre orientation and flexural behaviour of FRC, Mater. Struct. 41 (2007) 189-196.

[22] J.L. Chermant, L. Chermant, M. Coster, A.S. Dequiedt, C. Redon, Some field of applications of automatic image analysis in civil engineering, Cem. Concr. Compos. 23 (2001) 157-169.

[23] H.W. Reinhardt, C.U. Grosse, B. Weiler, Material characterization of steel fibre reinforced concrete using neutron CT, ultrasound and quantitative acoustic emission techniques. NDT International, 6 (2001) No.5.

[24] M. Faifer, R. Ottoboni, S. Toscani, L. Ferrara, Nondestructive testing of steel-fiber-reinforced concrete using a magnetic approach, IEEE Trans. Instrum. Meas. 60 (2011) 1709-1717.

[25] W. Rasband, ImageJ, National Institutes of Health, USA, 2008.http://rsb.info.nih.gov/ij/

[26] V.M.C.F. Cunha, Steel fibre reinforced self-compacting concrete-from micromechanics to composite behaviour, PhD thesis, University of Minho, Guimaraes, Portugal, 2010.

[27] L. Ferrara, N. Ozyurt, M. di Prisco, High mechanical performance of fiber reinforced cementitious composites - the role of casting-flow induced fiber orientation, Mater. Struct. , 44 (2011) 109-128.

[28] V.M.C.F. Cunha, J.A.O. Barros, J.M. Sena-Cruz, Pullout behaviour of Steel Fibres in Self Compacting Concrete, ASCE J. Mater. Civ. Constr. 22 (2010) 1-9.

[29] S.P. Timoshenko, J.N. Goodier, Theory of Elasticity, McGraw-Hill, New York,1991.

[30] C. Rocco, G. Guinea, L. Planas, M. Elices, Mechanisms of rupture in splitting tests, ACI Mater. J. 96 (1999) 52-60.

[31] J.A.O. Barros, Technology, design and applications of steel fibre reinforced self-compacting concrete, 6th International Conference Fibre Concrete 2011 - Technology, Design, Application, CTU in Prague, Masarykovakolej, 8 and 9 September 2011, (Invited Keynote Lecturer).

[32] P. Stroeven, J. Hu, Effectiveness near boundaries of fibre reinforcement in concrete, Mater. Struct. 39 (2006) 1001-1013.

[33] P. Soroushian, C.D. Lee, Distribution and orientation of fibers in steel fiber reinforced concrete, ACI Mater.J. 87 (1990) 433-439.

[34] V.M.C.F. Cunha, J.A.O. Barros, J.M. Sena-Cruz, An integral approach for modeling the tensile behaviour of steel fibre reinforced self-compacting concrete, Cem. Concr. Res. 41 (2011) 64-76.

[35] Y.T. Zhu, W.R. Blumenthal, T.C. Lowe, Determination of non-symmetric 3-D fibre-orientation distribution and average fibre length in short-fiber composites, J. Compos. Mater. 31 (1997) 1287-1301.

[36] F. Laranjeira, S. Grunewald, J. Walraven, C. Blom, C. Molins, A. Aguado, Characterization of the orientation profile of steel fiber reinforced concrete, Mater. Struct. 14 (2010) 1093-1111.

[37] C.V.S. KamerwaraRao, Effectiveness of random fibres in composites, Cem. Concr. Res. 9 (1979) 685-693.

[38] P. Stroeven, J. Hu, Effectiveness near boundaries of fibre reinforcement in concrete, Mater. Struct. 39 (2006) 1001-1013.

FIGURES AND TABLES

List of Figures:

Fig. 1 - Core extracting plan: (a) panel A, (b) panel B.

Fig. 2 - Schematic representation of the prismatic specimen production from an extracted core (dimensions are in mm).

Fig. 3 - Geometry of the specimen and setup of the splitting tensile test (dimensions are in mm): (a) specimen front view (top of the panel), (b) specimen lateral view and (c) LVDT connection detail.

Fig. 4 - Uniaxial tensile test setup: (a) specimen front view, (b) specimen lateral view, (c) LVDT connection detail.

Fig. 5 -Image processing steps: (a) converting a colored image to greyscale image (b) adjusting a threshold, (c) defining mask, noise (remove small noises) and watershed (separated fibres that are stuck together) functions, (d) fitting the best ellipse to each fibre.

Fig. 6 - Nominal tensile stress – crack opening width relationship, $\sigma - w$, obtained from splitting tensile test for: (a) θ=0° and (b) θ = 90°.

Fig. 7 - Nominal tensile stress – crack opening width relationship, $\sigma - w$, obtained from splitting tensile test for the two sides (top and bottom) of the specimens: (a) θ = 0° and (b) θ = 90°.

Fig. 8 - Uniaxial tensile stress – crack width relationship, σ - w: (a) θ = 0° and (b) θ = 90°.

Fig. 9 - Uniaxial tensile post-cracking parameters versus splitting tensile post cracking parameters: (a) Residual stress and (b) Fracture energy.

Fig. 10 - Localization of the plane surface considered in the fibre distribution assessment (units in mm).

Fig. 11 - Predicted orientation profile: (a) θ = 0° and (b) θ = 90°.

Fig. 12 - Explanation for fibre alignment in flowing concrete of a panel casting from the centre.

Fig. 13 - Relationship between the number of fibres in the fracture surfaces and the distance from the centre.

Fig. 14 - Categories of uniaxial tensile stress – crack width relationships, σ - w, : (a) $\eta_\theta \geq 0.80$ and $N^f_{eff} \geq 1.20$, (b) $0.68 < \eta_\theta < 0.80$ and $0.41 < N^f_{eff} < 1.20$, (c) $\eta_\theta \leq 0.68$ and $N^f_{eff} \leq 0.41$.

Fig. 15 - Orientation factor, η_θ, versus number of the effective fibres, N^f_{eff} .

List of Tables:

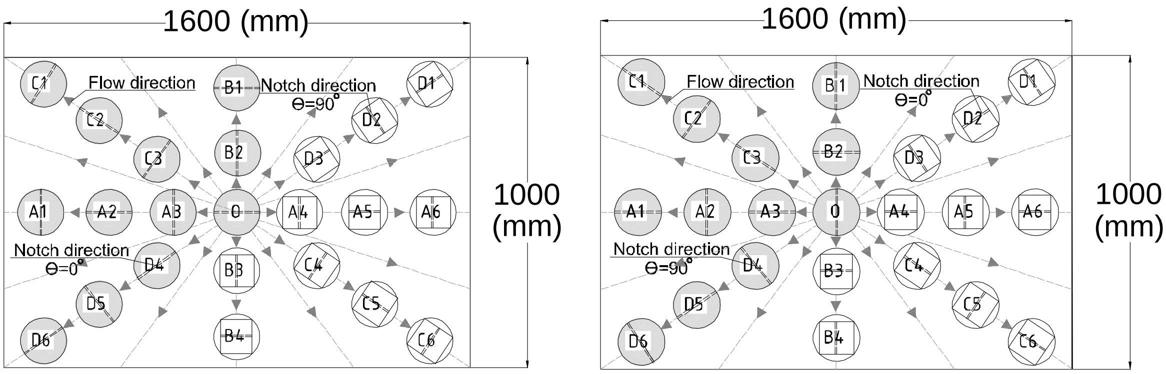

(a) (b)

Fig. 1 - Core extracting plan: (a) panel A, (b) panel B.

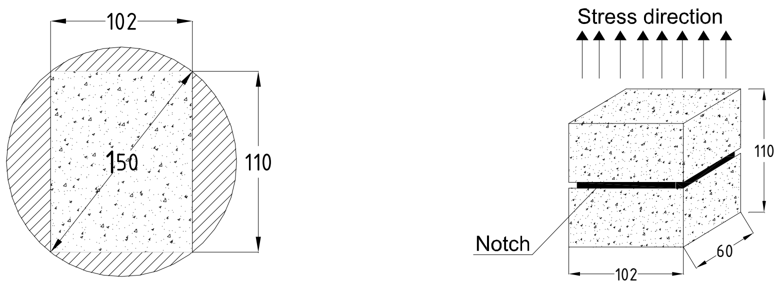

Fig. 2 - Schematic representation of the prismatic specimen production from an extracted core (dimensions are in mm).

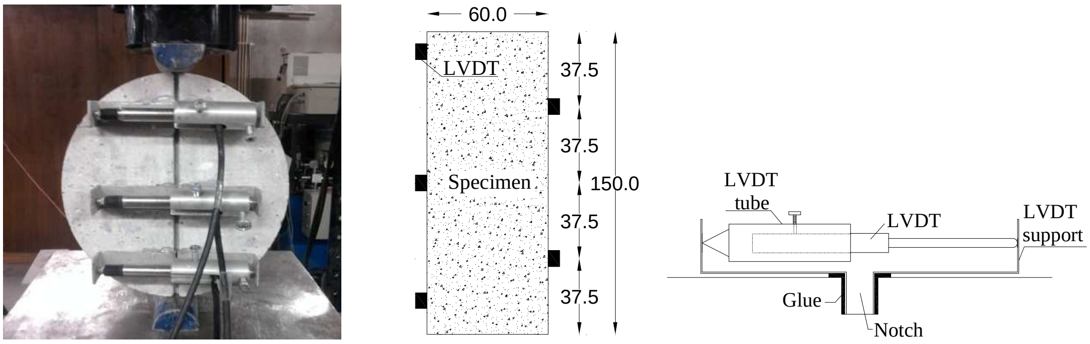

(a) (b) (c)

Fig. 3 - Geometry of the specimen and setup of the splitting tensile test (dimensions are in mm): (a) specimen front view (top of the panel), (b) specimen lateral view and (c) LVDT connection detail.

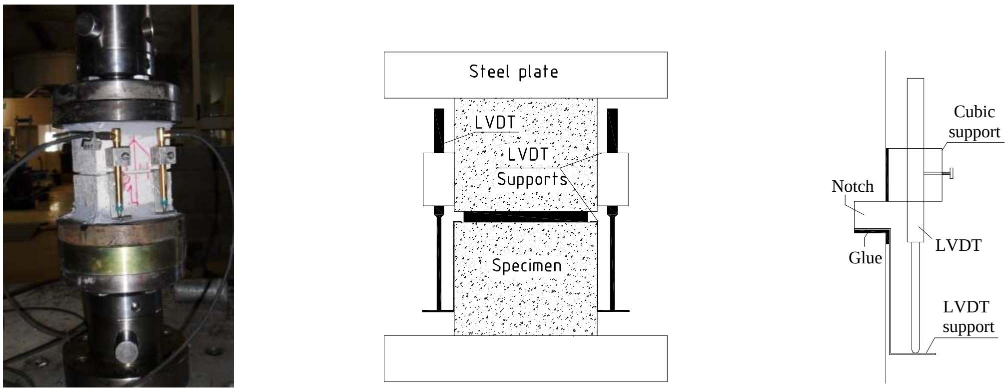

(a) (b) (c)

Fig. 4 - Uniaxial tensile test setup: (a) specimen front view, (b) specimen lateral view, (c) LVDT connection detail.

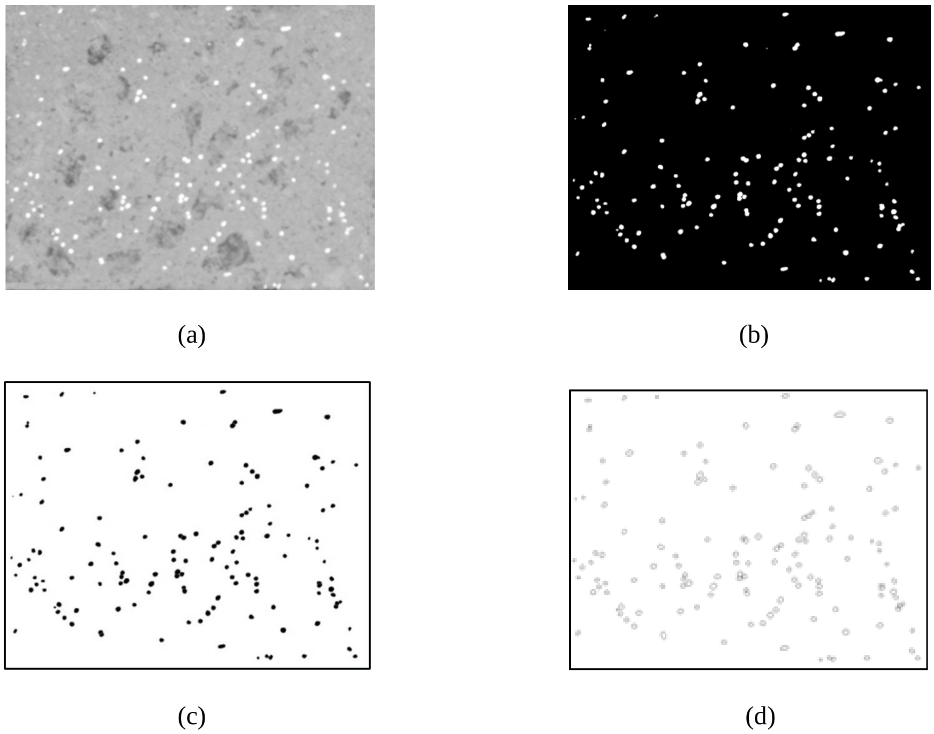

Fig. 5 - Image processing steps: (a) converting a colored image to greyscale image (b) adjusting a threshold, (c) defining mask, noise (remove small noises) and watershed (separated fibres that are stuck together) functions, (d) fitting the best ellipse to each fibre.

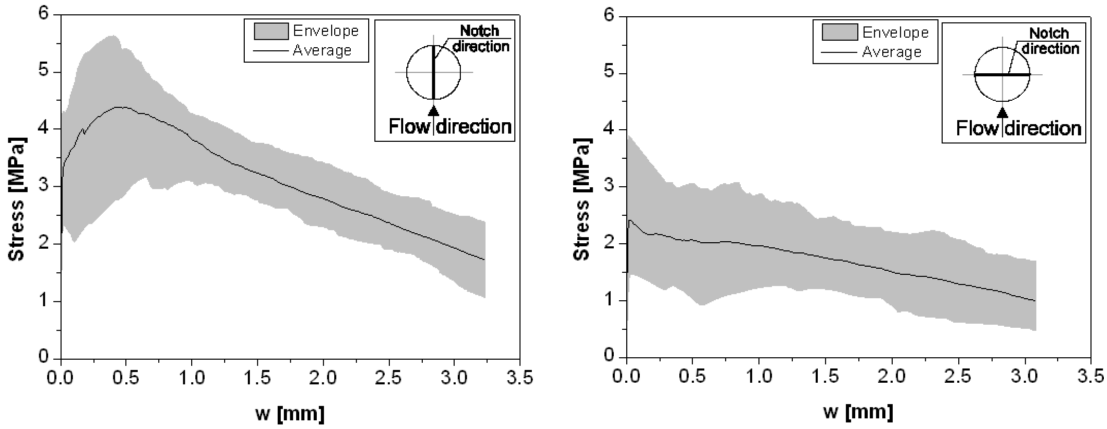

(a) (b)

Fig. 6 - Nominal tensile stress – crack opening width relationship, $\sigma - w$, obtained from splitting tensile test for: (a) θ=0˚ and (b) θ = 90˚.

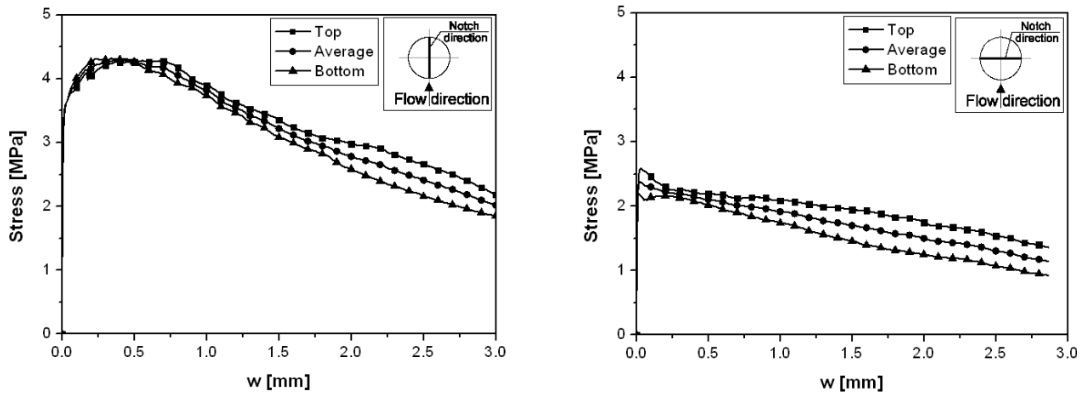

(a) (b)

Fig. 7 - Nominal tensile stress – crack opening width relationship, $\sigma - w$, obtained from splitting tensile test for the two sides (top and bottom) of the specimens: (a) $\theta = 0^{\circ}$ and (b) $\theta = 90^{\circ}$.

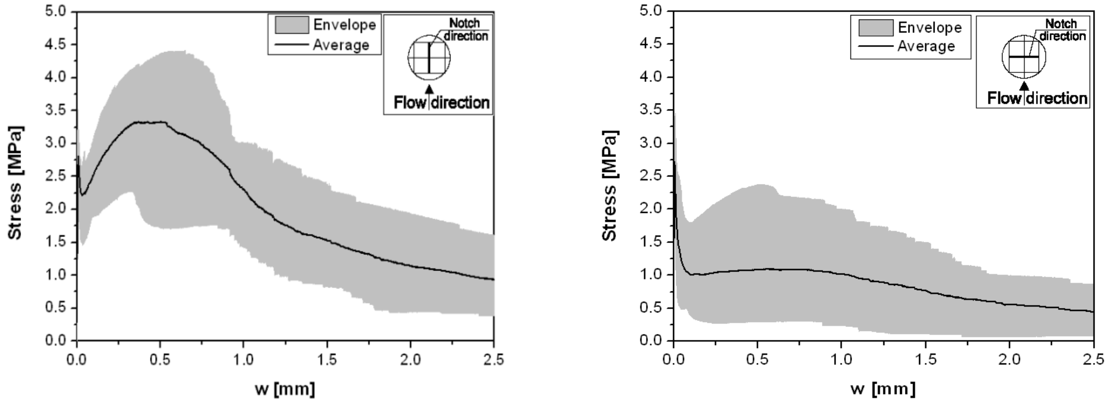

(a) (b)

Fig. 8 - Uniaxial tensile stress – crack width relationship, σ - w: (a) $\theta = 0^{\circ}$ and (b) $\theta = 90^{\circ}$.

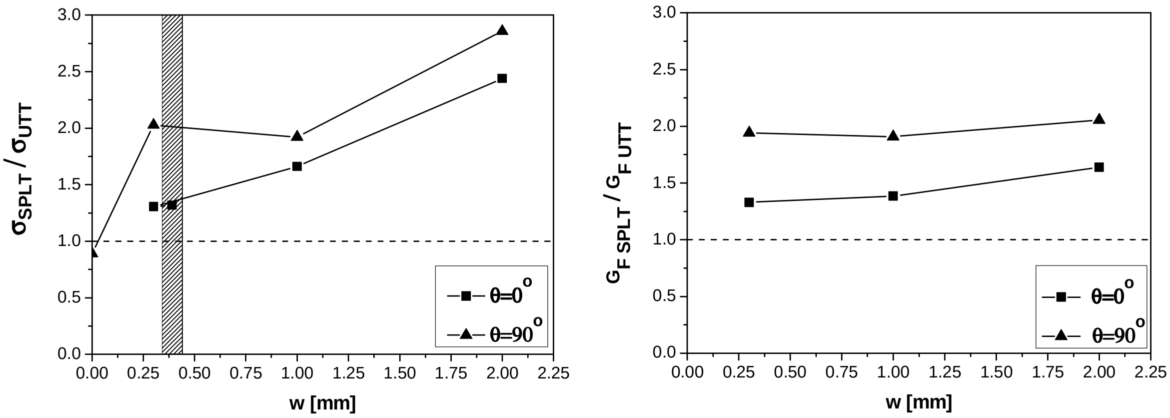

(a) (b)

Fig. 9 - Uniaxial tensile post-cracking parameters versus splitting tensile post cracking parameters: (a) Residual stress and (b) Fracture energy.

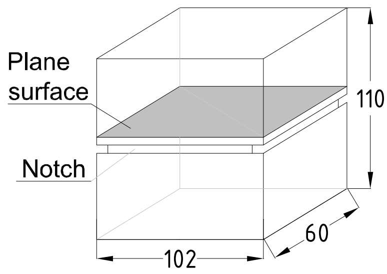

Fig. 10 - Localization of the plane surface considered in the fibre distribution assessment (units in mm).

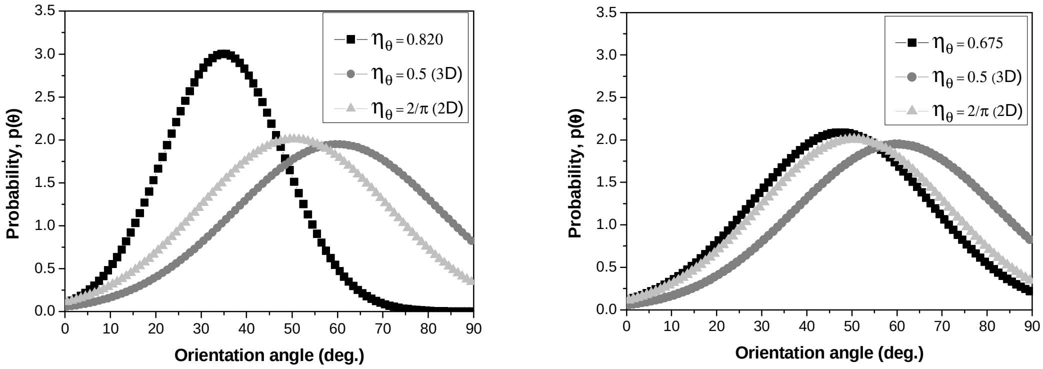

(a) (b)

Fig. 11 - Predicted orientation profile: (a) θ = 0° and (b) θ = 90°.

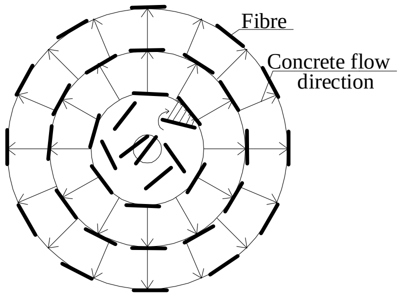

Fig. 12 - Explanation for fibre alignment in flowing concrete of a panel casting from the centre.

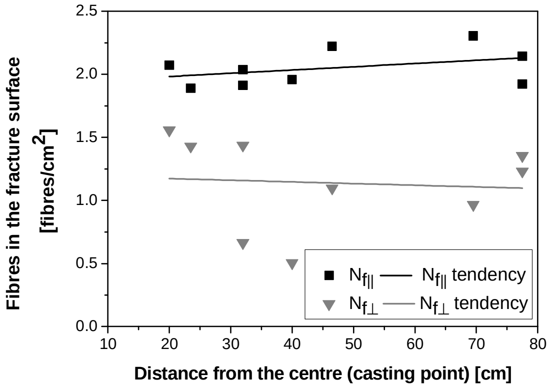

Fig. 13 - Relationship between the number of fibres in the fracture surfaces and the distance from the centre.

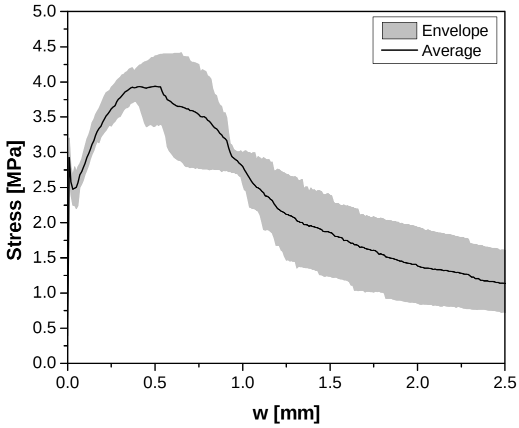

(a)

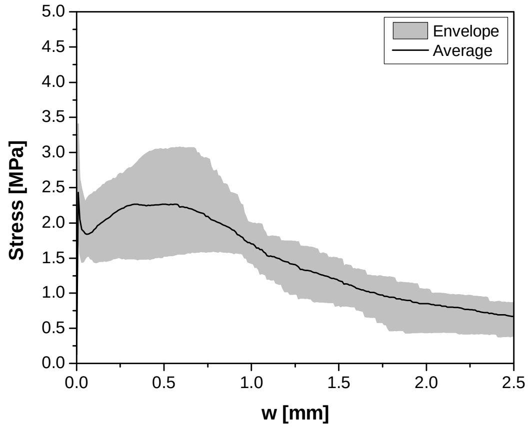

(b)

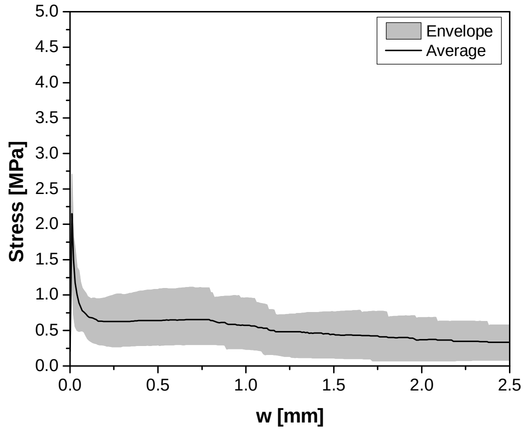

(c)

Fig. 14 - Categories of uniaxial tensile stress – crack width relationships, σ - w, : (a) $\eta_\theta \geq 0.80$ and $N_{eff}^{f} \geq 1.20$, (b) $0.68 < \eta_\theta < 0.80$ and $0.41 < N_{eff}^{f} < 1.20$, (c) $\eta_\theta \leq 0.68$ and $N_{eff}^{f} \leq 0.41$.

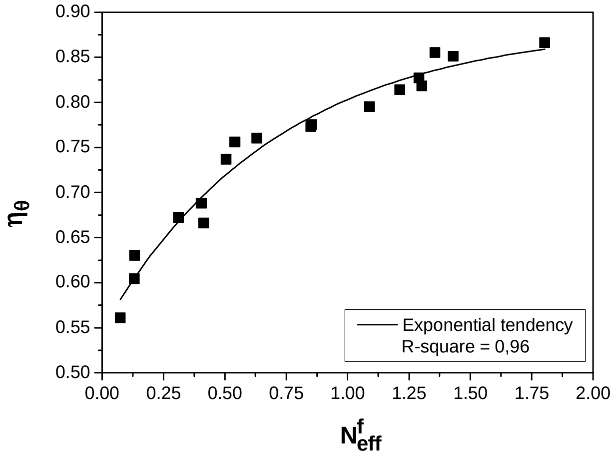

Fig. 15 - Orientation factor, η_θ, versus number of the effective fibres, N_{eff}^{f} .

Table 1- Mix proportions of steel fibre reinforced self-compacting concrete per m^3.

Cement [kg]	Water [kg]	W/C [–]	SP [kg]	Filler [kg]	Fine sand [kg]	Coarse sand [kg]	Coarse aggregate [kg]	Fibre [kg]
413	140	0.34	7.83	353	237	710	590	60

Table 2 - Residual stress and toughness parameters obtained from splitting and direct tensile tests.

	Series	Parameter	σ_{peak} [MPa]	$\sigma_{0.3}$ [MPa]	σ_1 [MPa]	σ_2 [MPa]	G_{F1} [N/mm]	G_{F2} [N/mm]
Splitting tensile test	θ = 0º ($\sigma_{\|\|}$)*	Average	4.39	4.23	3.82	2.79	4.07	7.32
		CoV(%)	25.6	29.7	24.3	30.2	27.2	25.2
		$K_{95\%}$	3.52	3.16	2.09	1.95	3.36	6.08
	θ = 90º ($\sigma_{\perp}$)*	Average	2.47	2.13	1.96	1.50	2.08	3.82
		CoV(%)	33.1	48.6	37.9	35.3	35.9	33.2
		$K_{95\%}$	2.07	1.74	1.46	1.09	1.49	2.83
Uniaxial tensile test	θ = 0º ($\sigma_{\|\|}$)*	Average	3.33	3.24	2.30	1.14	2.94	4.47
		CoV(%)	19.0	21.4	27.4	39.8	24.2	23.7
		$K_{95\%}$	3.10	2.73	1.83	0.80	2.42	3.72
	θ = 90º ($\sigma_{\perp}$)*	Average	2.72	1.05	1.02	0.56	1.09	1.86
		CoV(%)	19.1	64.5	65.4	57.1	59.6	59.9
		$K_{95\%}$	2.34	0.51	0.48	0.30	0.57	0.96

[*] || and ⊥- notch direction parallel (θ = 0º) and perpendicular (θ = 90º) to the concrete flowdirection, respectively.

Table 3- Fibre distribution parameters.

		θ = 0°				θ = 90°			
Specimen	Distance [cm]	N^f [fibres/cm^2]	N^f_{eff} [fibres/cm^2]	η_θ [-]	ξ_{seg} [-]	N^f [fibres/cm^2]	N^f_{eff} [fibres/cm^2]	η_θ [-]	ξ_{seg} [-]
B3	20.0	2.071	1.291	0.827	0.580	1.557	0.405	0.688	0.476
A4	23.5	1.889	1.356	0.855	0.518	1.430	0.506	0.737	0.510
C4	32.0	2.036	1.430	0.851	0.555	0.665	0.133	0.630	0.597
D3	32.0	1.913	0.853	0.775	0.491	1.436	0.415	0.666	0.586
B4	40.0	1.956	0.851	0.773	0.530	0.506	0.074	0.561	0.643
A5	46.5	2.220	1.212	0.814	0.479	1.097	0.311	0.672	0.725
A6	69.5	2.304	1.803	0.866	0.557	0.967	0.132	0.604	0.539
C6	77.5	2.142	1.303	0.818	0.600	1.232	0.541	0.756	0.485
D1	77.5	1.921	1.089	0.795	0.532	1.355	0.631	0.760	0.594
Average		2.050	1.24	0.820	0.538	1.138	0.35	0.675	0.573
CoV (%)		7.16	23.74	4.15	7.33	31.98	57.11	10.20	14.00